Electronic Supplementary Information (ESI)

rtl-M-MOFs (M = Cu, Zn) with a T-shaped bifunctional pyrazole-isophthalate ligand showing flexibility and S-shaped Type F-IV sorption isotherms with high saturation uptakes for M = Cu

Simon Millan,[a] Beatriz Gil-Hernández,[b] Erik Milles,[a] Serkan Gökpinar,[a] Gamall Makhloufi,[a] Alexa Schmitz,[a] Carsten Schlüsener[a] and Christoph Janiak*[a]

[a] Institut für Anorganische Chemie und Strukturchemie, Heinrich-Heine Universität Düsseldorf, 40204 Düsseldorf, Germany. *E-Mail: janiak@hhu.de
[b] Departamento de Química, Facultad de Ciencias de La Laguna, Sección Química, Universidad de La Laguna, 38206, La Laguna, Tenerife, Spain

Emails:
simon.millan@hhu.de; beagher@ull.edu.es; erik.milles@hhu.de; serkan.goekpinar@hhu.de; gamall.makhloufi@hhu.de; alexa.schmitz@hhu.de; carsten.schluesener@hhu.de

Table of contents

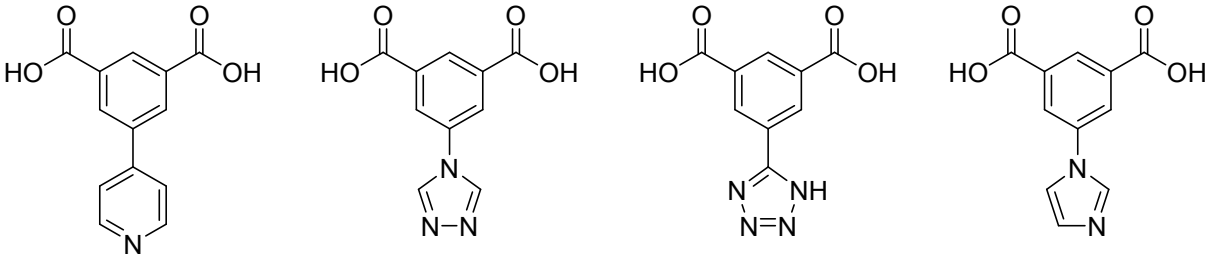

1 **2** **3** **4**

Scheme S1 Exemplary examples of T-shaped ligands reported in the literature for the construction of rtl-MOFs with the heterocycles pyridine (1),[1] triazole (2),[2,3] tetrazole (3)[4] and imidazole (4)[5] as the pillaring functionality.

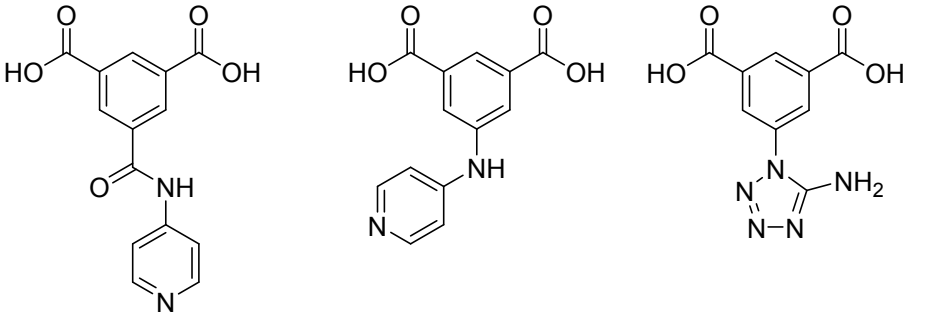

5 **6** **7**

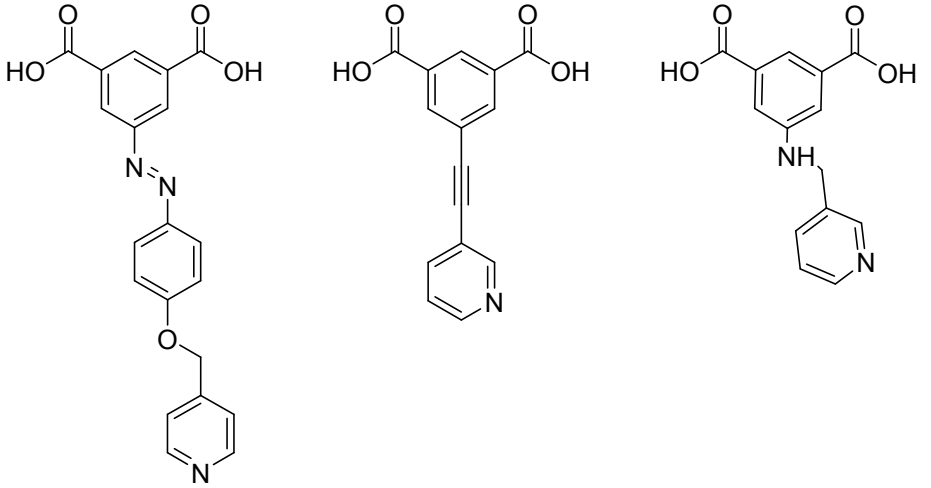

8 **9** **10**

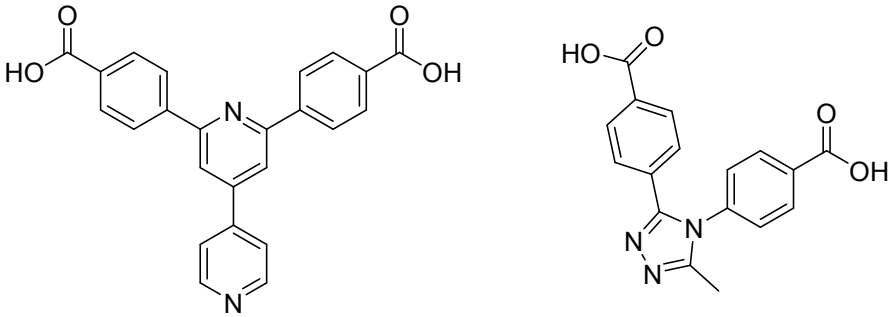

11 **12**

Scheme S2 Exemplary functionalized T-shaped ligands **5** (**eea**),[6,7,8,6] (**rtl**),[7] **7** (**apo**),[9] **8** (**eea**)[2], **9** (**eea**)[10], **10** (**eea**),[10] **11** (**pyr**)[11] and **12** (**rtl**)[12] (topology abbreviation in parentheses).

Synthetic procedures for the ligand H_3Isa-az-dmpz

Dimethyl 5-(2-(3-pentan-2,4-dionyl)hydrazono)isophthalate:

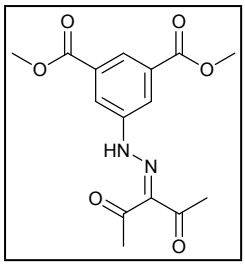

In the first step the diazonium salt was synthesized conforming to the classical procedures followed by a Japp-Klingemann reaction with acetylacetone. [13,14] Therefore 4.18 g (20.0 mmol) of dimethyl 5-aminoisophthalate were suspended in 40 mL of 3 mol/L HCl at 0 °C. $NaNO_2$ (1.38 g, 20.0 mmol, 1 eq) dissolved in 10 mL of de-ionized water (DI-H_2O) was slowly added via a dropping funnel. The solution of the diazonium salt was added to an ice bath cooled solution of acetylacetone (2.1 mL, 20.0 mmol), NaOH (1.07 g, 26.8 mmol) and NaOAc (8.18, 99.7 mmol) in 160 mL of MeOH and 160 mL of DI-H_2O. The solution was stirred for 0.5 h at 0 °C and afterwards for 1 h at room temperature. The yellow powder was collected by suction and dried in air. The product was recrystallized from ethanol (420 mL) and was kept for crystallization overnight in the refrigerator. The fibrous yellow product was collected by suction (5.04 g, 15.7 mmol, 79 %).

^{1}H-NMR (300 MHz, $CDCl_3$, δ [ppm]): 14.68 (s, 1H, NH), 8.44 (t, J = 1.51 Hz, 1H, Ar H), 8.19 (d, J = 1.51 Hz, 2H, Ar H), 3.96 (s, 6H, -CH_3), 2.60 (s, 6 H, -CH_3), 2.51(s, 6 H, -CH_3).
^{13}C-NMR (75 MHz, $CDCl_3$, δ [ppm]): 198.58, 197.08, 165.60, 142.40. 134.20, 132.29, 127.17, 120.91, 52.81, 31.85, 26.80.
ESI-MS: $[M+H]^+$ 321.1, $[2M+H+K]^{2+}$ 340.1
EA [%] calc. for $C_{15}H_{16}N_2O_6$ C 56.25, H 5.04, N 8.75; found C 56.31, H 4.93, N 8.64.

Dimethyl 5-(4-(3,5-dimethyl-1H-pyrazolyl)azo)isophthalate:

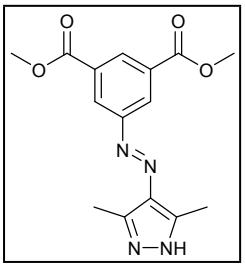

To a solution of dimethyl 5-(2-(3-pentan-2,4-dionyl)hydrazono)isophthalate (2.00 g, 6.25 mmol) in EtOH (100 mL) hydrazine hydrate (304 µl, 6.25 mL, 1 eq) was added and the mixture was refluxed for 4h. The solution was concentrated under reduced pressure and quenched with DI-H_2O. The yellow powder was collected by suction an dried overnight at 65 °C in a vacuum oven to yield 1.92 g (6.07 mmol, 97 %). The product was used without further purification.

^{1}H-NMR (300 MHz, DMSO-d_6, δ [ppm]): 12.95 (s, 1H, NH), 8.35 (d, J = 1.37 Hz, 2H, Ar H), 8.26 (t , J = 1.37 Hz, 1 H, Ar H), 3.89 (*s*, 6H, -CH_3), 2.48 (s, 3H, -CH_3), 2.37 (s, 3H, -CH_3).
^{13}C-NMR (75 MHz, DMSO-d_6, δ [ppm]): 164.94, 153.01, 142.97, 139.67, 134.27, 131.09, 129.35, 125.54.
ESI-MS: $[M+H]^+$ 317.3
EA [%] calc. for $C_{15}H_{16}N_4O_4$ C 56.96, H 5.10, N 17.71; found C 57.12, H 5.03, N 17.73.

5-(4-(3,5-Dimethyl-1H-pyrazolyl)azo)isophthalic acid (H_3Isa-az-dmpz):

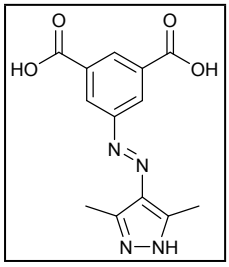

Dimethyl 5-(4-(3,5-dimethyl-1H-pyrazolyl)azo)isophthalate (1.84 g, 5.8 mmol) was dissolved in 105 mL of MeOH, 27 mL of DI-H_2O and 6.4 g (114mmol) of KOH and refluxed for 24 h. The MeOH was removed under reduced pressure. The remaining yellow solution was adjusted to pH 3 with 1N HCl. The yellow precipitate was collected with suction, washed with DI-H_2O and dried at 80 °C in a vacuum oven (1.64 g, 5.97 mmol, 98%).

^{1}H-NMR (600 MHz, DMSO-d_6, δ [ppm]): 13.27 (s, 3H, NH/COOH), 8.46 (t, J = 1.60 Hz, 1H, Ar H), 8.38 (d, J = 1.60 Hz, 2H, Ar H), 2.47 (s, 6H, -CH_3).
^{13}C-NMR (150 MHz, DMSO-d_6, δ [ppm]): 166.27, 153.18, 141.29, 134.39, 132.40, 130.05, 125.62, 12.01.
ESI-MS: $[M+H]^+$ 289,3
EA [%] calc. for H_3Isa-az-dmpz·0.5H_2O $C_{15}H_{16}N_4O_4$ C 52.53, H 4.41, N 18.85; found C 52.22, H 4.22, N 18.72.

NMR-Spectroscopy

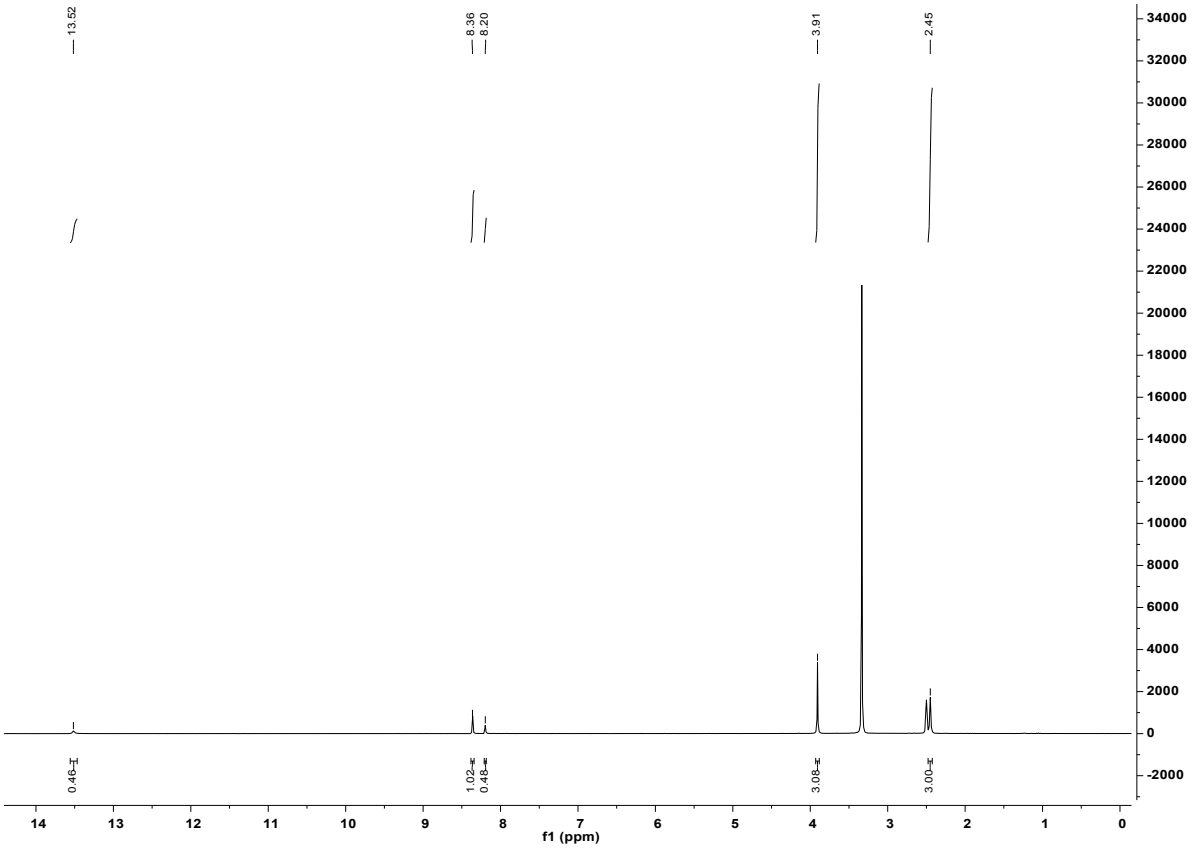

Figure S1 ^{1}H-NMR spectrum Me_2HIsa-az-acac in DMSO-d_6

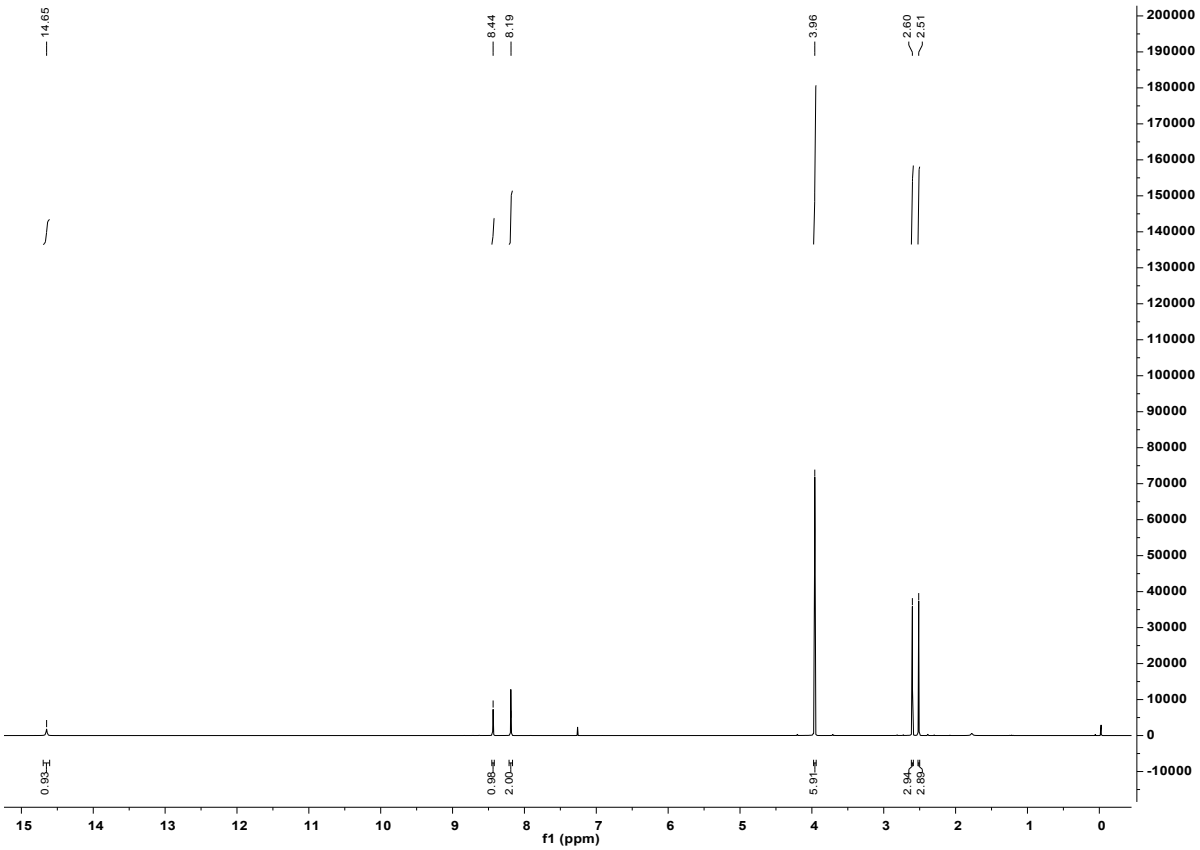

Figure S2 ^{1}H-NMR spectrum Me_2HIsa-az-acac in $CDCl_3$.

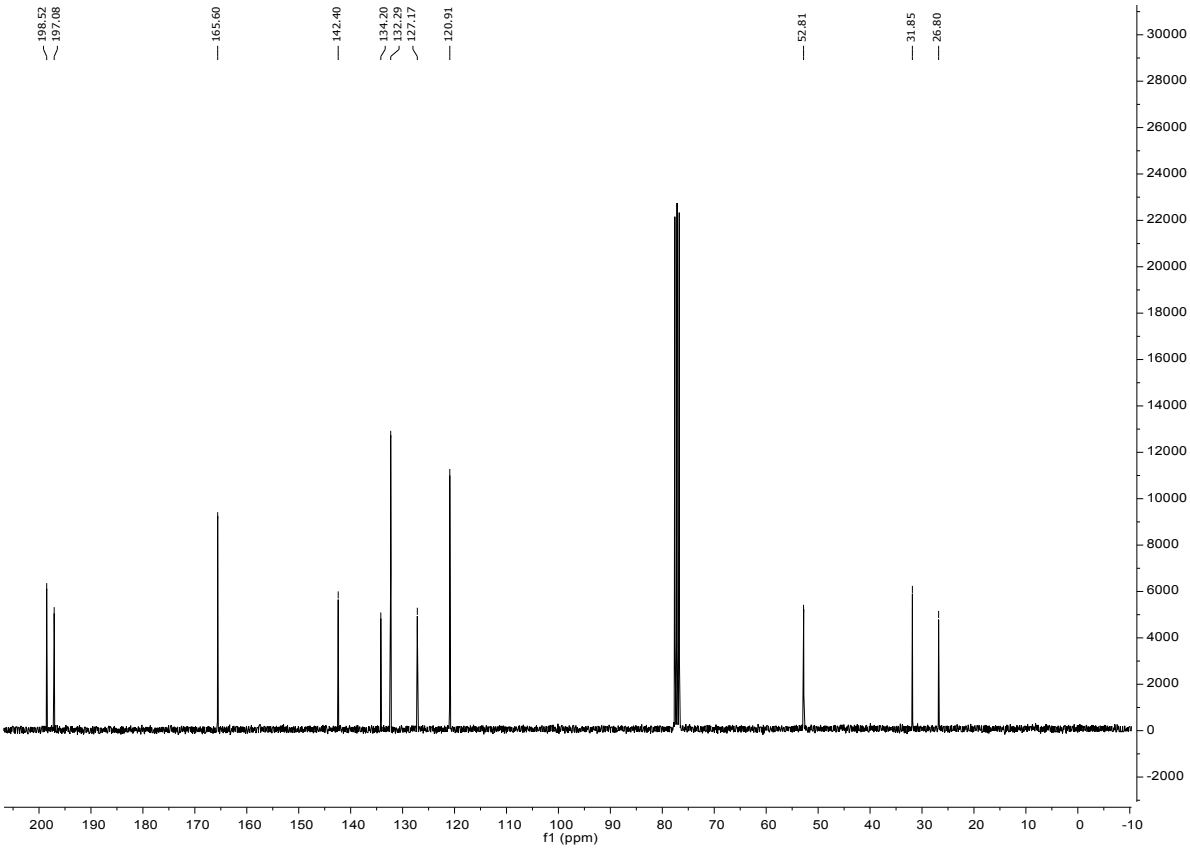

Figure S3 ^{13}C-NMR spectrum of Me_2HIsa-az-acac in $CDCl_3$.

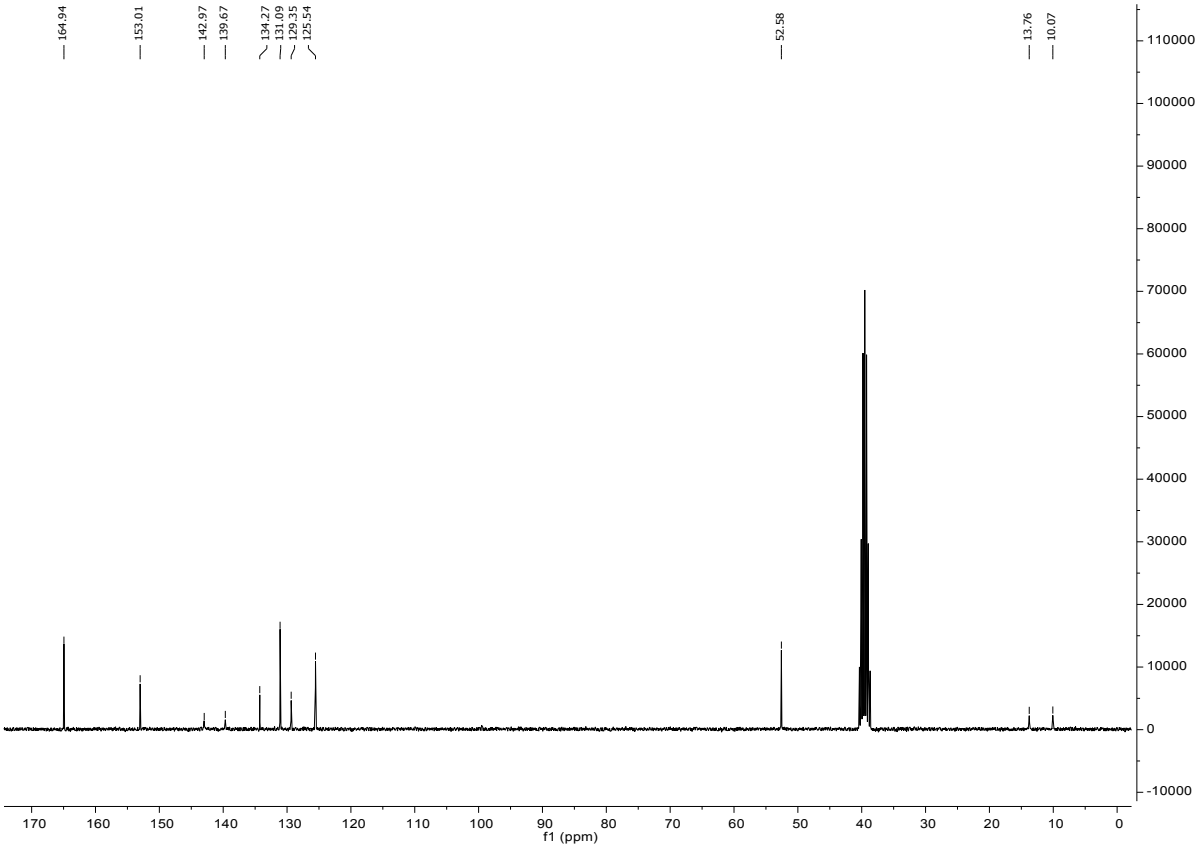

Figure S4 ^{13}C-NMR spectrum of Me_2HIsa-az-dmpz in DMSO-d_6.

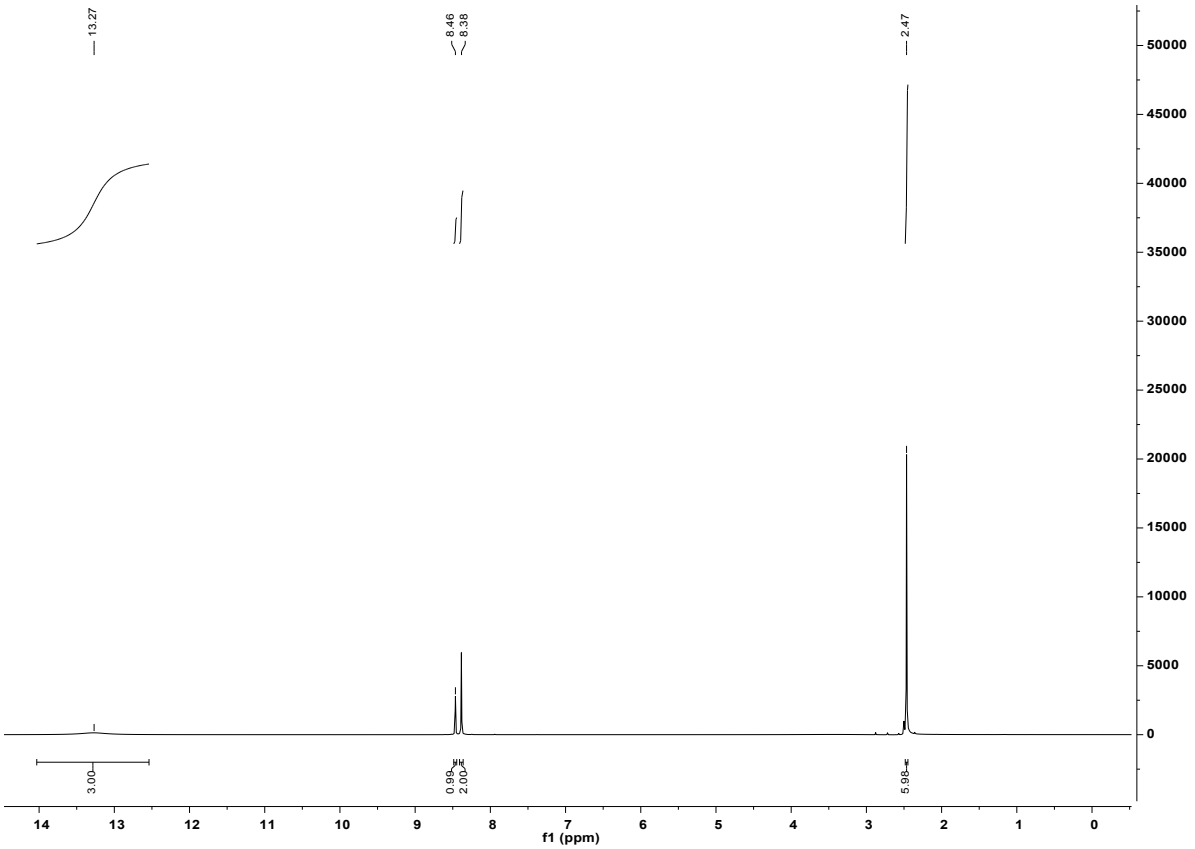

Figure S5 ^{1}H-NMR spectrum H_3Isa-az-dmpz in DMSO-d_6.

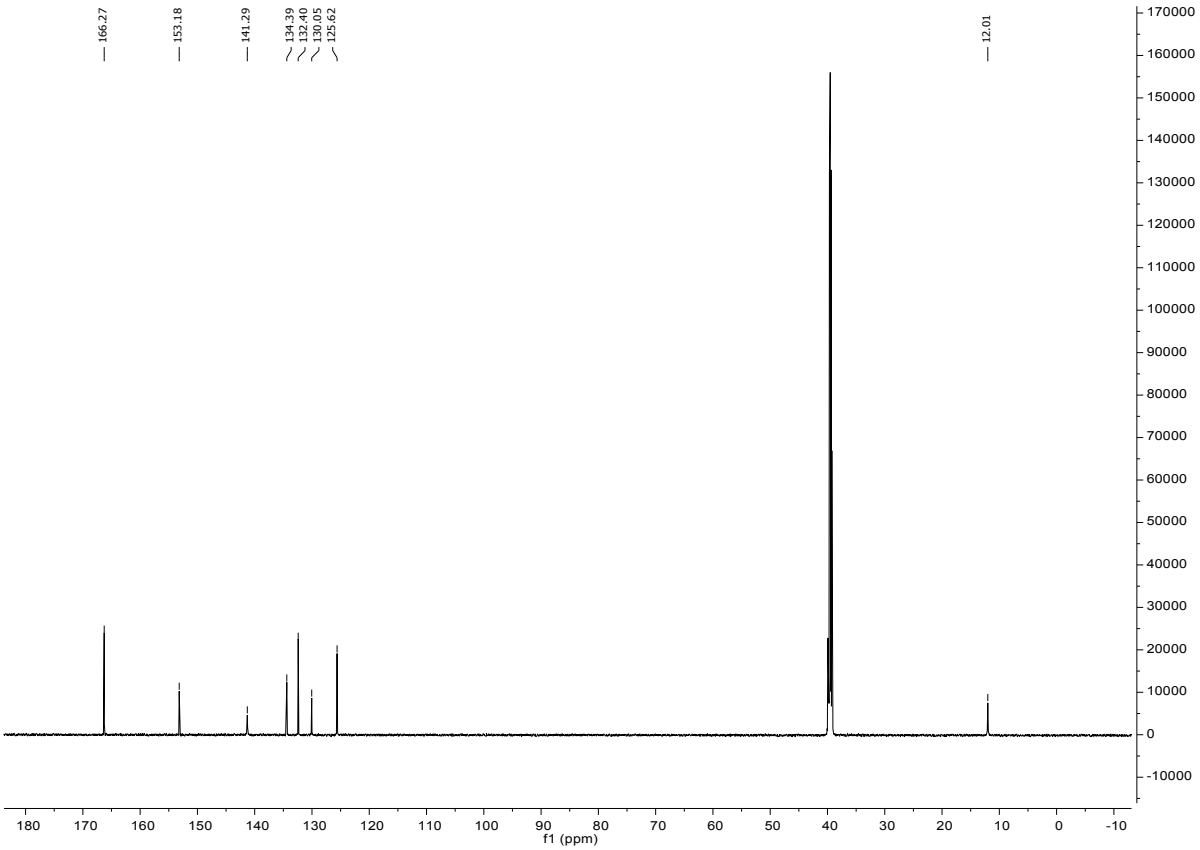

Figure S6 ^{13}C-NMR spectrum of H_3Isa-az-dmpz in DMSO-d_6.

Asymmetric unit of rtl-[ZnHIsa-az-dmpz]·(DMF)$_2$

In **rtl**-Zn, one of the DMF molecules can be described as disordered, as shown in Fig. S7b.

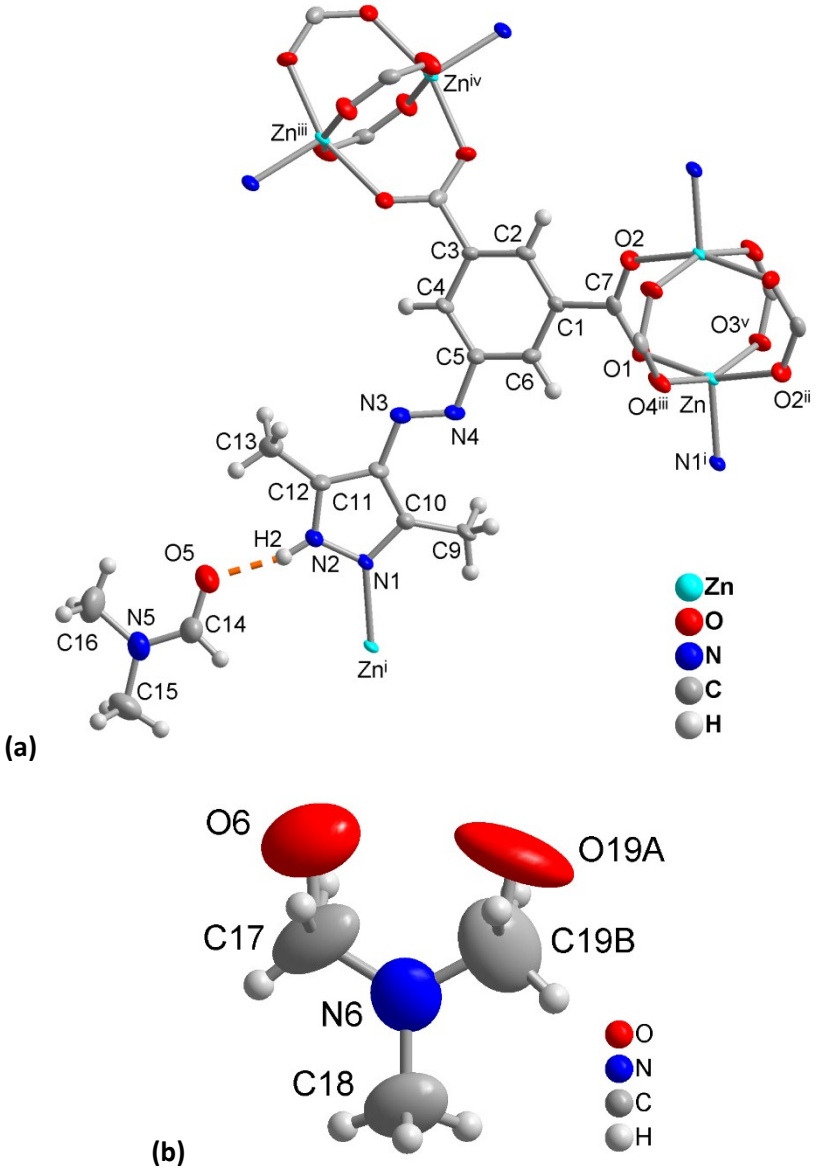

Figure S7 (a) Extended asymmetric unit of **rtl**-[ZnHIsa-az-dmpz]·(DMF)$_2$ (50% thermal ellipsoids; the disordered DMF-molecule is omitted for clarity). Symmetry transformations: i -x+2, -y, -z+1; ii -x+1, -y, -z+1;; iii x, -y-1/2, z+1/2; iv -x+1, y+1/2, -z+1/2; v -x+1, y-1/2, -z+1/2. Details of hydrogen bond N2-H2···O5 (orange-dashed line): N2-H2 0.831(1) Å, H2···O5 1.85(2) Å, N2···O5 2.656(5) Å, N2-H2···O5 164(4)°.

(b) Disorder of the "free", non-hydrogen-bonded DMF solvent molecule.

Characterization of the phases during the activation process of rtl-[CuHIsa-az-dmpz].

^{1}H-NMR auf digested MOF samples

For the ^{1}H-NMR experiments 10 mg of the MOF sample were suspended in 0.7 mL DMSO-d_6 and digested by the addition of 20 µL of DCl (37% in D_2O).

Complete exchange of DMF against acetone in **rtl**-Cu-acetone can be assumed from the absence of the aldehyde signal (7.94 ppm) and the methyl groups (2.70 ppm, 2.86 ppm) (Figure S8 and S9). The NMR spectrum of the digested sample after supercritical drying **rtl**-Cu-scd indicates that there is still one acetone molecule per formula unit retained in the framework.

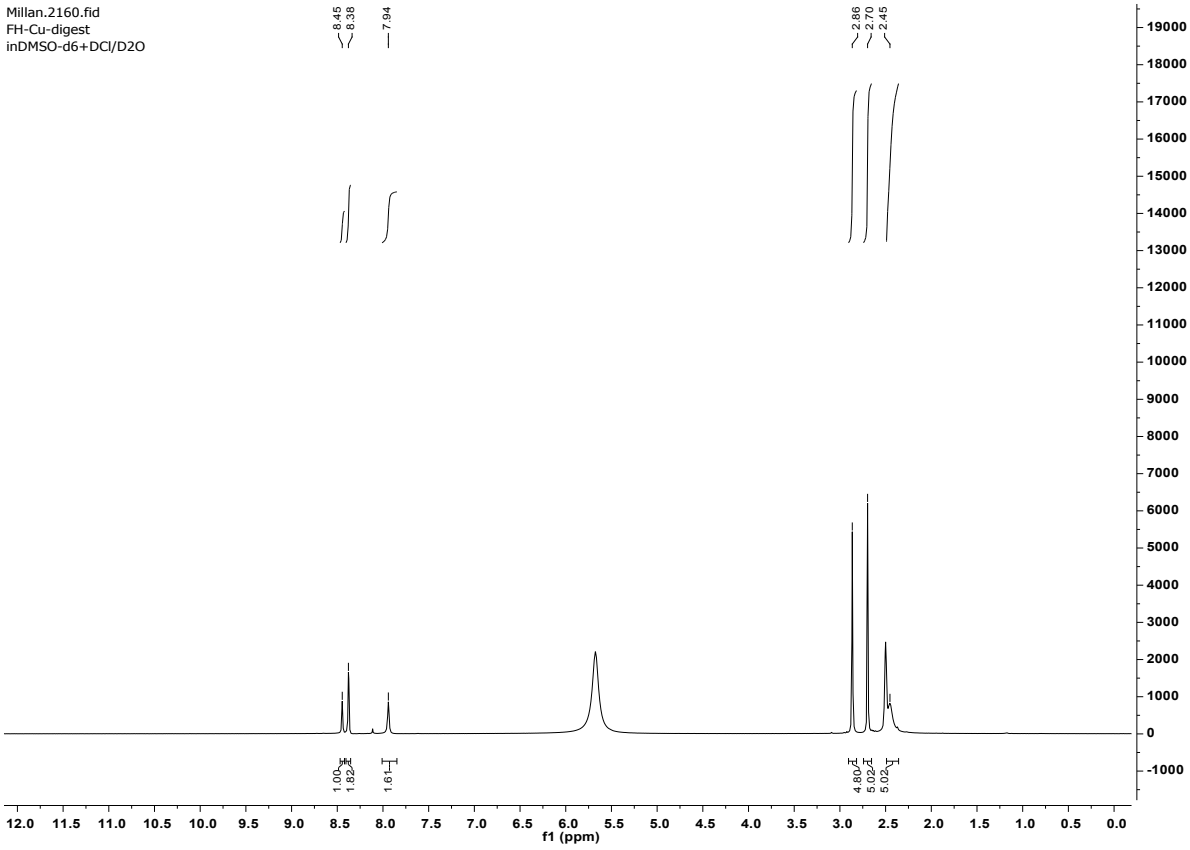

Figure S8 ^{1}H-NMR spectrum of digested **rtl**-Cu-as in DMSO-d_6/DCl.

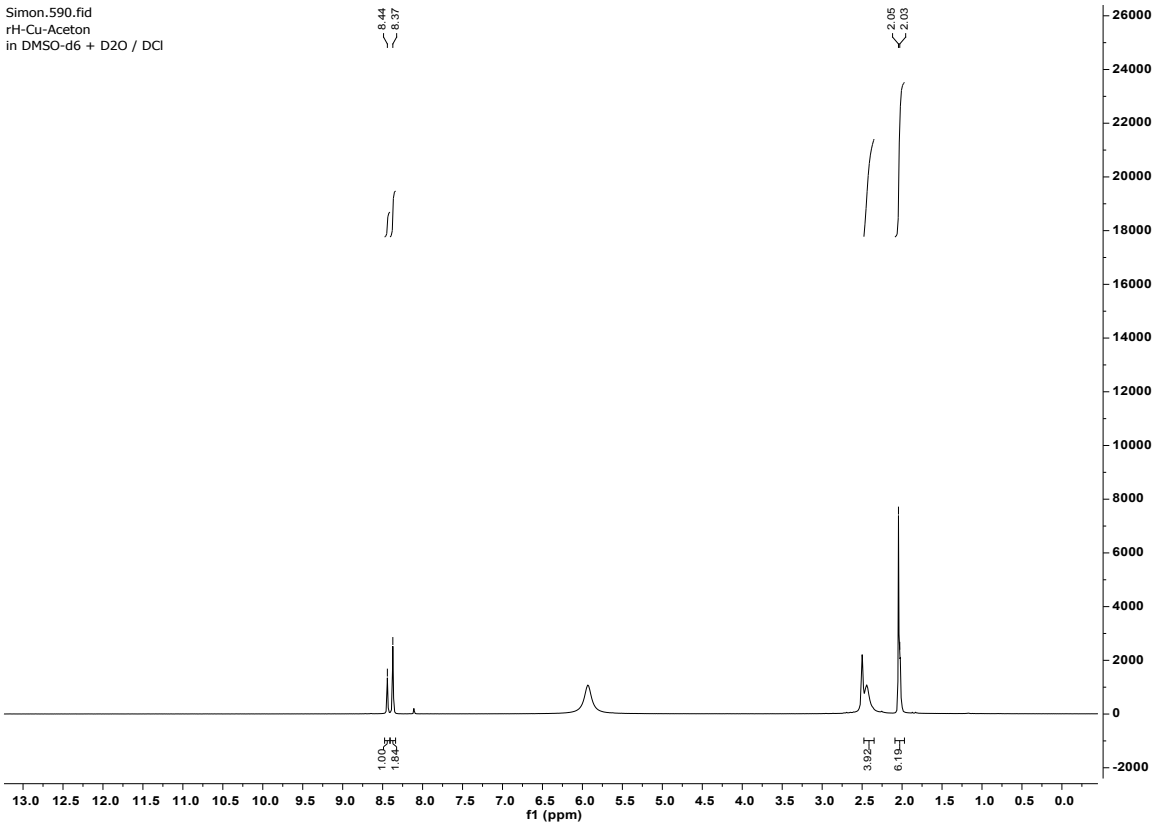

Figure S9 ^{1}H-NMR spectrum of digested **rtl**-Cu-acetone in DMSO-d_6/DCl.

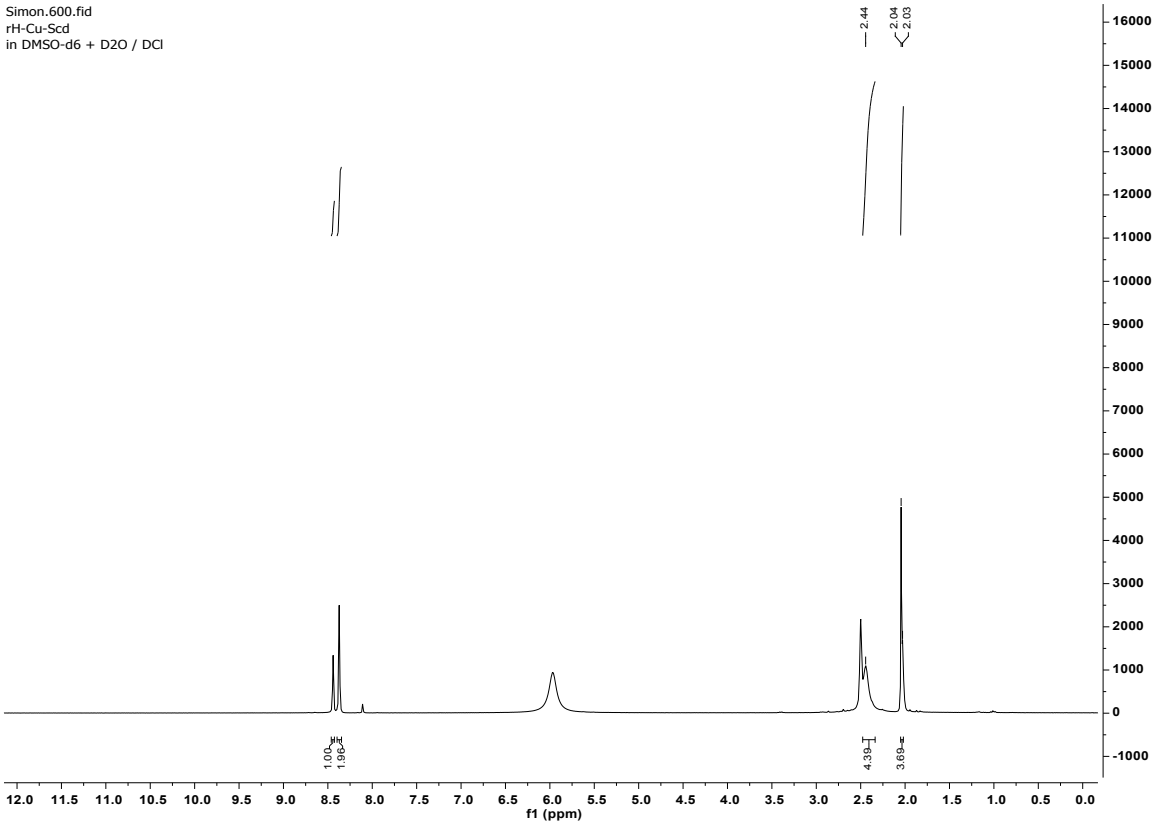

Figure S10 ^{1}H-NMR spectrum of digested **rtl**-Cu-scd in DMSO-d_6/DCl.

Thermogravimetric Analysis (TGA)

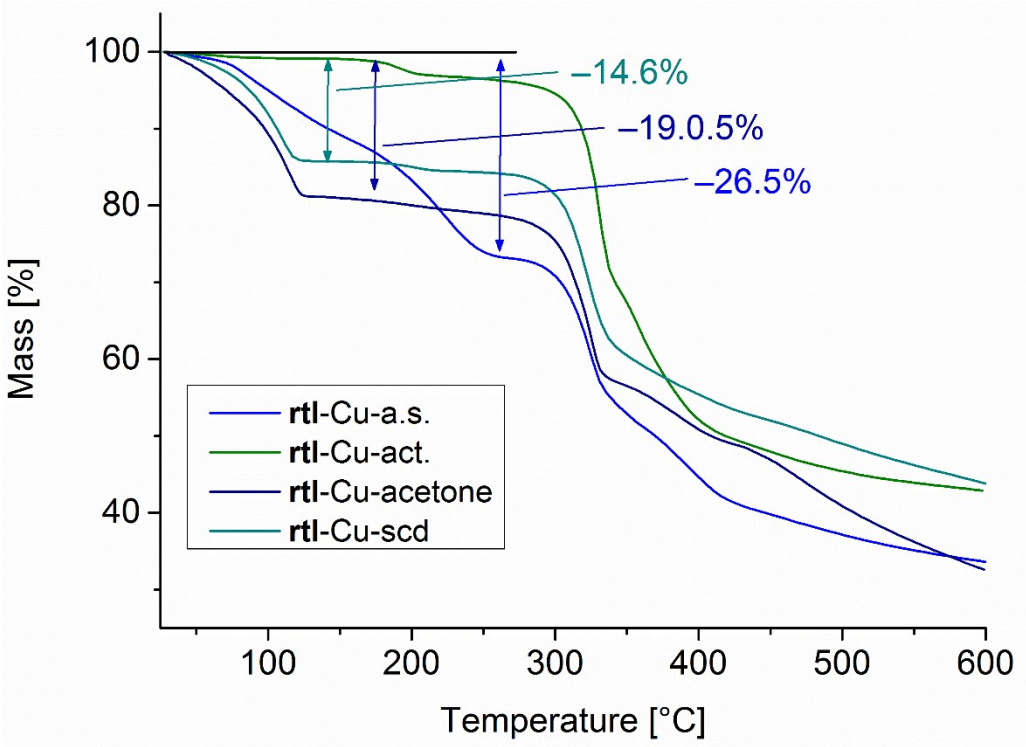

Figure S11 TGA curves of the as-synthesized (a.s.), activated (act.), acetone-exchanged (acetone) and the supercritically-dried (scd) materials of **rtl**-[CuHIsa-az-dmpz] (a.s.: blue, act.: green, acetone: marine blue, scd: dark cyan).

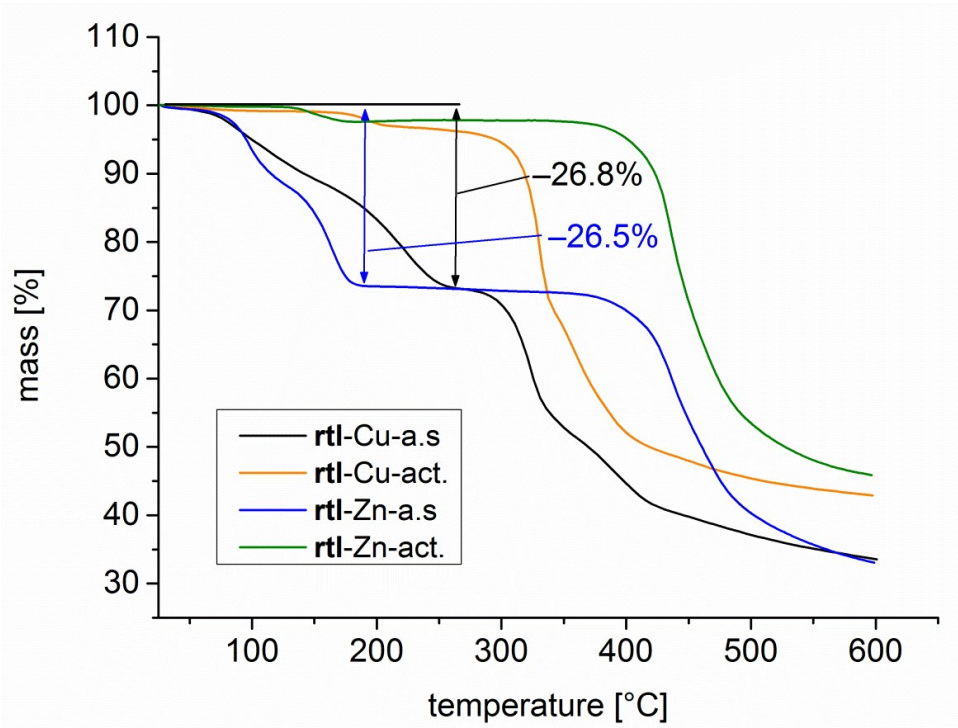

Figure S12 TGA curves of the as-synthesized (a.s.) and activated (act.) materials for **rtl**-[CuHIsa-az-dmpz] (a.s: black, act.: orange) and **rtl**-[Zn(HIsa-az-dmpz)] (a.s.: blue, act.: green) in the temperature range 25 – 600 °C with heating rate of 5 $Kmin^{-1}$ under nitrogen atmosphere.

Optical images

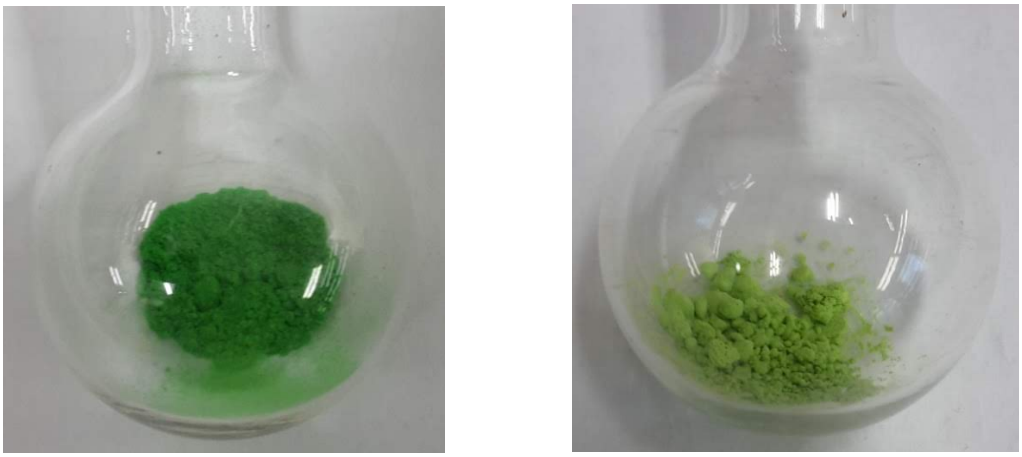

Figure S13 Optical photographs of the grass green open form of **rtl**-[CuHIsa-az-dmpz] after supercritical drying (right) and the yellow-green closed form [CuHIsa-az-dmpz]-act (left) after activation at 120 C.

FT-IR spectroscopy

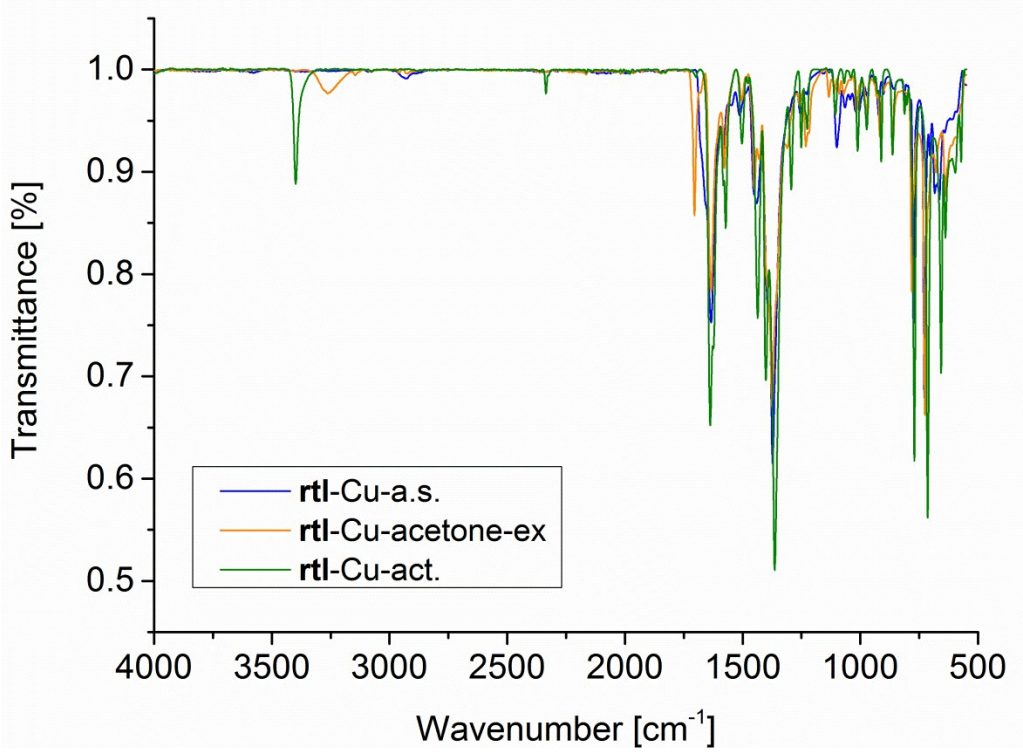

Figure S14 FT-IR spectra of **rtl**-[Cu(HIsa-az-dmpz)]-a.s. (blue), **rtl**-[Cu(HIsa-az-dmpz)]-acetone-exchanged (orange) and **rtl-**[Cu(HIsa-az-dmpz)]-act. (green).

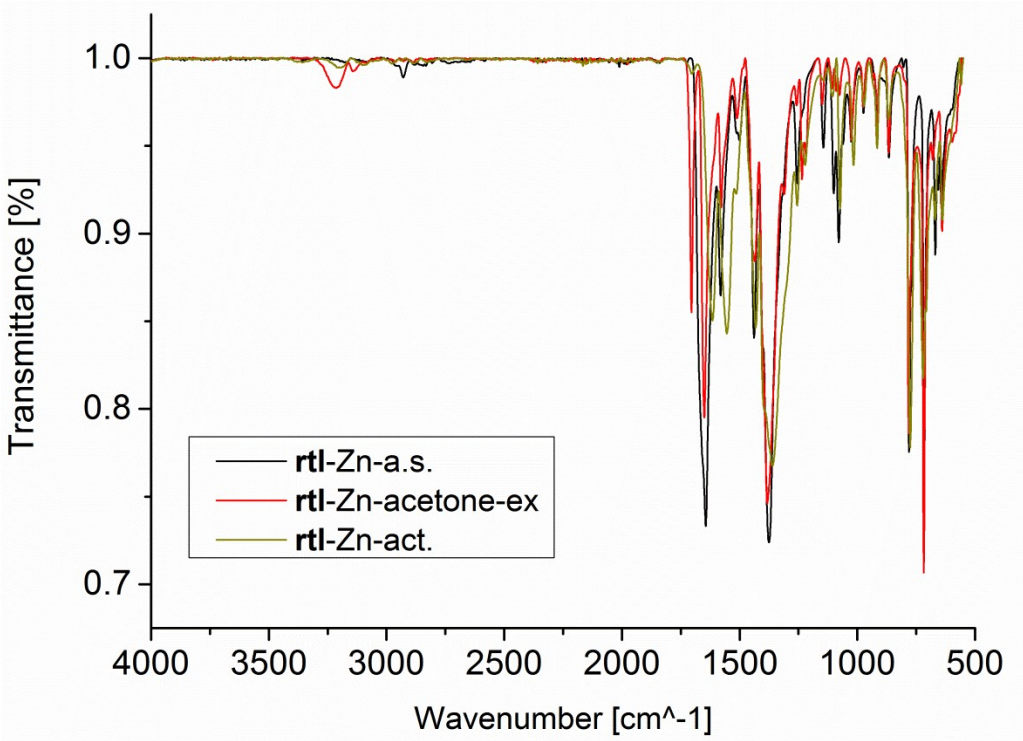

Figure S15 FT-IR spectra of **rtl**-[Zn(HIsa-az-dmpz)]-a.s. (black), **rtl**-[Zn(HIsa-az-dmpz)]-acetone-exchanged (red) and **rtl-**[Zn(HIsa-az-dmpz)]-act. (olive-green).

Scanning electron microscopy (SEM)

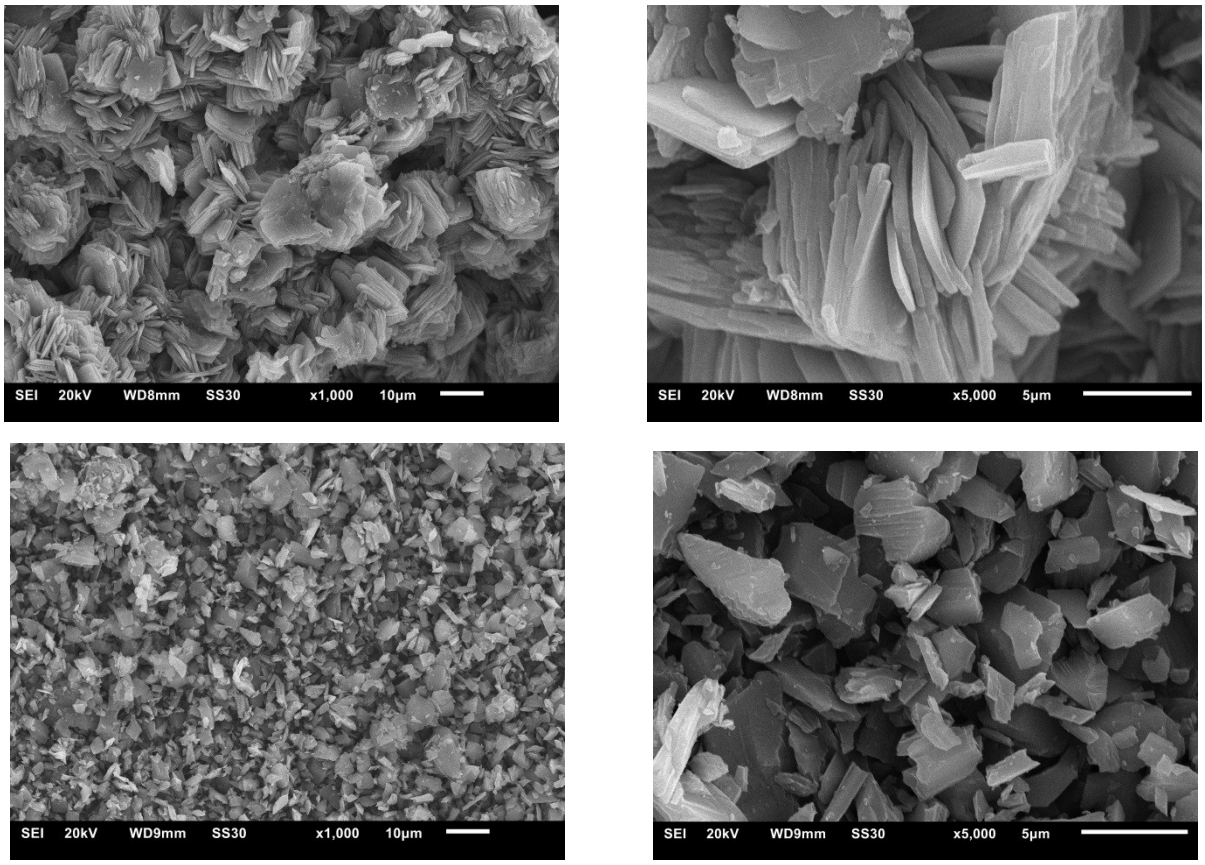

Figure S16 SEM images for **rtl**-[Cu(HIsa-az-dmpz)]-a.s (top) and **rtl-**[Cu(HIsa-az-dmpz)]-act. (bottom).

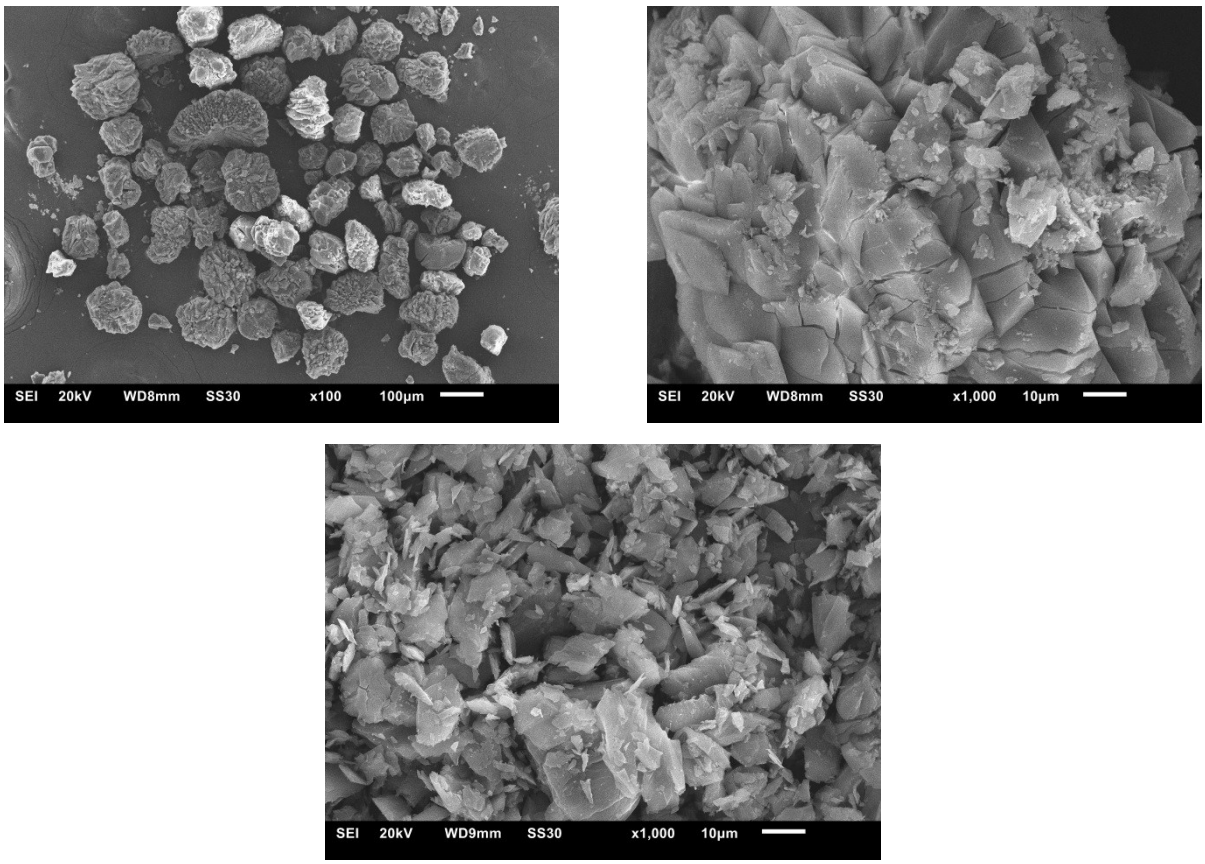

Figure S17 SEM images for **rtl**-[Zn(HIsa-az-dmpz)]-a.s (top) and **rtl**-[Zn(HIsa-az-dmpz)]-act. (bottom).

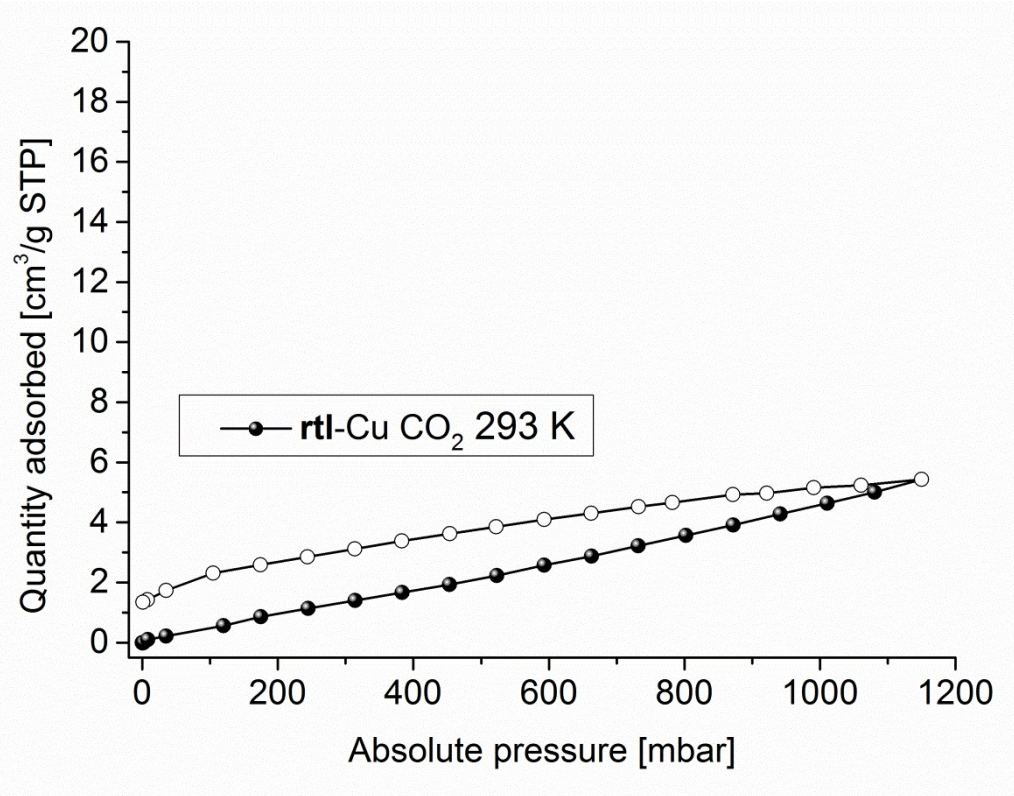

Figure S18 Sorptiom isotherm of **rtl**-[Cu(HIsa-az-dmpz)]-act. for CO_2 at 293 K in the low pressure range between 0–1 bar.

Theoretical surface area and pore volume of rtl-[Cu(HIsa-az-dmpz)]

The theoretical pore volumes and surface areas were calculated with the programs Mercury[15,16], Platon[17,18] and CrystalExplorer[1920], respectively.

Mercury 'Void' calculation	
Probe radius 1.2 Å, grid spacing 0.7 Å Void volume [Å^3] (% of unit cell) specific [cm^3/g]	 859.73 (40.6) 0.37
Probe radius 0.7 Å, grid spacing 0.2 Å Void volume [Å^3] (% of unit cell) specific [cm^3/g]	 1081.79 (51.0) 0.47
Platon 'Calc Void'	
Total Potential Solvent Area [Å^3] (% of unit cell) specific [cm^3/g]	969.8 (45.7) 0.42
CrystalExplorer calculation	
Surface area $S_{Unit\ Cell}$ (isovalue 0.002) [Å^2] specific [m^2/g]	782 3367
Surface area $S_{Unit\ Cell}$ (isovalue 0.003) [Å^2] specific [m^2/g]	595 2561
Pore Volume (isovalue 0.002) [Å^3] Specific [cm^3/g]	981 0.42
Pore Volume (isovalue 0.0003) [Å^3] Specific [cm^3/g]	579 0.35
Experimental gas uptake	
Langmuir surface area [m^2/g] Pore Volume N_2 @77 K [cm^3/g]	1610 0.55
Langmuir surface area [m^2/g] Pore Volume CO_2 @195 K [cm^3/g]	1440 0.57
Pore Volume CO_2 @298 K [cm^3/g]	0.47

Theoretical specific pore volumes are calculated according to (Void Volume x N_A)/(Z x M_{AU}) or (SAV x N_A)/(Z x M_{AU})
Theoretical specific surface areas are calculated according to ($S_{Unit\ Cell}$ x N_A)/(Z x M_{AU})
Experimental pore volumes are calculated under the assumption of the validity of the Gurvich rule[21] according to (specific amount adsorbed)/(density of liquid adsorbate) with ρ_{N2} = 0.808 g/cm^3, ρ_{CO2} = 1.08 g/cm^3 and $\rho_{CO2,\ 298K}$ = 0.712 g/cm^3.

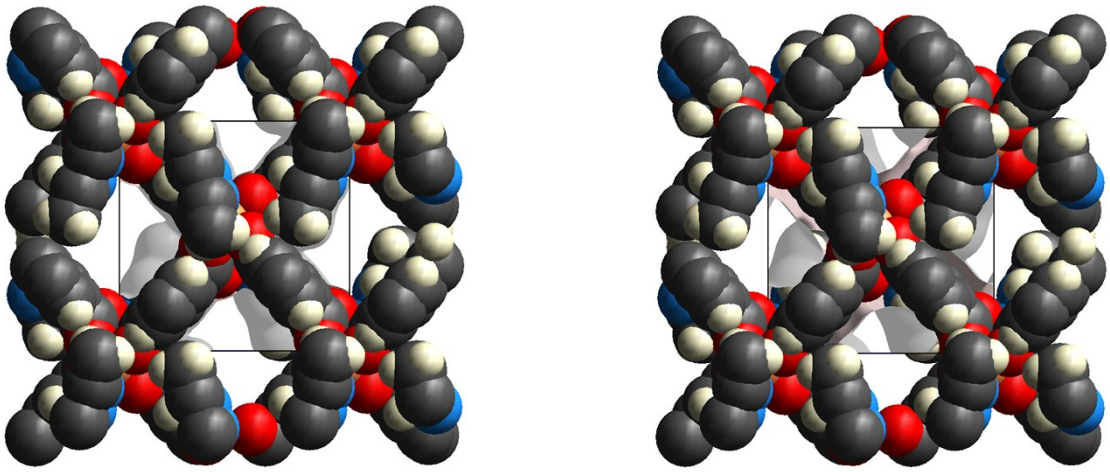

Figure S19 Illustration of the iso-surface area for **rtl**-[Cu(HIsa-az-dmpz)] at 0.002 e/Å^3 (left) and 0.0003 e/Å^3 right calculated with CrystalExplorer.

The measured pore volumes are slightly higher than the ones calculated from the DMF-filled single crystal structure data. But this comparison assumes that the (flexible) structure does not change during the sorption measurement. This retention of the solid-state X-ray structure framework is obviously not the case for **rtl**-[Cu(HIsa-az-dmpz)]. We expect that distortions of the framework have also a large impact on the theoretically calculated specific pore volumes. Concerning activation, we can state that the comparison between theoretical and experimental pore volumes indicates that the sample of **rtl**-[Cu(HIsa-az-dmpz)] became fully activated under the chosen activation protocol.

Langmuir Report rtl-[CuHIsa-az-dmpz] N_2@77 K 1st Cycle

Langmuir surface area: 1.610,1536 ± 2,3402 m²/g
Slope: 0,002703 ± 0,000004 g/cm³ STP
Y-intercept: 0,099 ± 0,002 mbarKg/cm³ STP
b: 0,027245 1/mbar
Qm: 369,9310 cm³/g STP
Correlation coefficient: 0.999986
Molecular cross-sectional area: 0.1620 nm²

Pressure [mbar]	Quantity Adsorbed [cm³/g STP]	P/Q [mbarJg/cm³ STP]
205.725744	312.0763	0.659
232.934491	319.3683	0.729
258.96383	325.3148	0.796
285.81555	326.6452	0.875
309.935032	330.1213	0.939
359.061293	336.0183	1.069
410.654068	340.5038	1.206
461.6057	343.6405	1.343
512.671174	346.2907	1.48
564.532562	347.4821	1.625
634.373514	348.7545	1.819
666.378214	350.3159	1.902
718.425215	351.6511	2.043
768.891129	352.9789	2.178
820.622157	354.3191	2.316
205.725744	312.0763	0.659
232.934491	319.3683	0.729
258.96383	325.3148	0.796
285.81555	326.6452	0.875
309.935032	330.1213	0.939
359.061293	336.0183	1.069
410.654068	340.5038	1.206
461.6057	343.6405	1.343
512.671174	346.2907	1.48
564.532562	347.4821	1.625
634.373514	348.7545	1.819
666.378214	350.3159	1.902
718.425215	351.6511	2.043
768.891129	352.9789	2.178
820.622157	354.3191	2.316

Langmuir Report rtl-[CuHIsa-az-dmpz] N_2@77 K 2nd Cycle

Langmuir surface area: 1.658,2486 ± 2,7142 m²/g
Slope: 0,002625 ± 0,000004 g/cm³ STP
Y-intercept: 0,101 ± 0,002 mbarNg/cm³ STP
b: 0,025926 1/mbar
Qm: 380,9808 cm³/g STP
Correlation coefficient: 0.999968
Molecular cross-sectional area: 0.1620 nm²

Pressure [mbar]	Quantity Adsorbed [cm³/g STP]	P/Q [mbarJg/cm³ STP]
204.200987	324.0059	0.63
230.721192	329.98	0.699
256.854119	334.1922	0.769
282.313722	336.0458	0.84
306.558478	338.1414	0.907
330.977862	340.535	0.972
356.518411	343.0431	1.039
381.47303	345.158	1.105
406.908688	347.0217	1.173
432.268832	348.7245	1.24
457.70152	350.4215	1.306
483.19239	352.0176	1.373
508.582072	353.4794	1.439
534.047798	354.555	1.506
559.259679	355.579	1.573
584.845838	356.632	1.64
610.273277	357.6296	1.706
635.663285	358.5215	1.773
661.021882	359.572	1.838
686.663253	360.4542	1.905
711.878063	361.3366	1.97
737.341958	362.1774	2.036
762.725863	363.0448	2.101
788.142968	363.8641	2.166
813.59189	364.6641	2.231
838.994511	365.5557	2.295

Langmuir Report rtl-[CuHIsa-az-dmpz] CO_2@195 K 1st Cycle

Langmuir surface area: 1.436,6883 ± 2,9633 m²/g
Slope: 0,003179 ± 0,000007 g/cm³ STP
Y-intercept: 0,046 ± 0,005 mbarJg/cm³ STP
b: 0,069834 1/mbar
Qm: 314,5445 cm³/g STP
Correlation coefficient: 0.999983
Molecular cross-sectional area: 0.1700 nm²

Pressure [mbar]	Quantity Adsorbed [cm³/g STP]	P/Q [mbarJg/cm³ STP]
399.120997	302.2214	1.321
466.781301	304.8239	1.531
533.931719	306.4843	1.742
599.864788	307.6665	1.950
666.998036	308.4912	2.162
733.270840	309.0442	2.373
800.040511	309.3462	2.586
866.724333	309.5878	2.800
940.091282	309.6250	3.036
1019.693559	309.6287	3.293

Langmuir Report rtl-[CuHIsa-az-dmpz] CO_2@195 K 2nd Cycle

Langmuir surface area: 1.447,3146 ± 2,5086 m²/g
Slope: 0,003156 ± 0,000005 g/cm³ STP
Y-intercept: 0,043 ± 0,004 mbarJg/cm³ STP
b: 0,073759 1/mbar
Qm: 316,8710 cm³/g STP
Correlation coefficient: 0.999989
Molecular cross-sectional area: 0.1700 nm²

Pressure [mbar]	Quantity Adsorbed [cm³/g STP]	P/Q [mbarJg/cm³ STP]
399.666362	305.4194	1.309
466.5052	307.7736	1.516
600.055406	310.1891	1.934
686.115609	311.1138	2.205
752.955993	311.5865	2.417
799.852213	311.9694	2.564
866.901402	312.1711	2.777
959.996144	312.2208	3.075
1019.742628	312.2971	3.265

Topology Analysis for [CuHIsa-az-dmpz] with ToposPro[22]

```
##########################################################
2:C13 H10 Cu N4 O4/intercluster bonds and atoms at rings>8
##########################################################


Topology for Ti1
--------------------
Atom Ti1 links by bridge ligands and has
Common vertex with                    R(A-A)
V  1    0.0000    0.5000    0.5000   ( 0 0 0)     5.320A       1
V  1    0.0000    0.0000    0.0000   ( 0-1 0)     5.360A       1
V  1    1.0000    0.5000    0.5000   ( 1 0 0)    10.043A       1
Topology for V1
--------------------
Atom V1 links by bridge ligands and has
Common vertex with                    R(A-A)
Ti 1   -0.2055    0.7105    0.7257   ( 0 1 1)     5.320A       1
Ti 1    0.2055    0.2895    0.2743   ( 0 0 0)     5.320A       1
Ti 1   -0.2055    0.7895    0.2257   ( 0 0 0)     5.360A       1
Ti 1    0.2055    0.2105    0.7743   ( 0 0 0)     5.360A       1
Ti 1    0.7945    0.7105    0.7257   ( 1 1 1)    10.043A       1
Ti 1   -0.7945    0.2895    0.2743   (-1 0 0)    10.043A       1
-------------------------
Structural group analysis
-------------------------


-------------------------
```

Structural group No 1

Structure consists of 3D framework with VTi2

Coordination sequences

Ti1: 1 2 3 4 5 6 7 8 9 10

Num 3 14 19 62 51 144 99 254 163 400

Cum 4 18 37 99 150 294 393 647 810 1210

V1: 1 2 3 4 5 6 7 8 9 10

Num 6 10 38 34 102 74 198 130 326 202

Cum 7 17 55 89 191 265 463 593 919 1121

TD10=1180

Vertex symbols for selected sublattice

Ti1 Point symbol:{4.6^2}

Extended point symbol:[4.6(2).6(2)]

V1 Point symbol:{4^2.6^10.8^3}

Extended point symbol:[4.4.6.6.6.6.6.6.6.6.6(2).6(2).8(2).8(4).8(4)]

Point symbol for net: {4.6^2}2{4^2.6^10.8^3}

3,6-c net with stoichiometry (3-c)2(6-c); 2-nodal net

Topological type: **rtl** rutile 3,6-conn (topos&RCSR.ttd) {4.6^2}2{4^2.6^10.8^3} - VS [4.4.6.6.6.6.6.6.6.6.6(2).6(2).*.*.*] [4.6(2).6(2)] (17085 types in 3 databases

Table S1. Selected Bond lengths [Å] and angles [°] for [Cu(HIsa-az-dmpz)]·(DMF)$_2$.

Cu—O1	1.929 (8)	C3—C4	1.433 (13)
Cu—O4^{i}	1.929 (8)	C3—C8	1.466 (14)
Cu—O3^{ii}	1.948 (6)	C4—C5	1.384 (13)
Cu—O2^{iii}	1.966 (7)	C5—C6	1.366 (13)
Cu—N1^{iv}	2.154 (8)	C9—C10	1.526 (13)
O1—C7	1.250 (11)	C10—C11	1.381 (14)
O2—C7	1.267 (12)	C11—C12	1.376 (15)
O3—C8	1.275 (13)	C12—C13	1.487 (17)
O4—C8	1.262 (12)	N4—C5	1.449 (12)
O5—C14	1.15 (2)	N5—C14	1.248 (18)
N1—N2	1.319 (11)	N5—C15	1.457 (19)
N1—C10	1.329 (12)	N5—C16	1.50 (2)
N2—C12	1.386 (14)	C1—C6	1.406 (14)
N2—H2N	0.8800	C1—C2	1.410 (13)
N3—N4	1.242 (11)	C1—C7	1.433 (14)
N3—C11	1.419 (13)	C2—C3	1.381 (13)
O1—Cu—O4^{i}	87.7 (3)	C5—C6—C1	122.2 (11)
O1—Cu—O3^{ii}	88.8 (3)	C5—C6—H6	118.9
O4^{i}—Cu—O3^{ii}	167.3 (3)	C1—C6—H6	118.9
O1—Cu—O2^{iii}	167.4 (3)	O1—C7—O2	127.8 (10)
O4^{i}—Cu—O2^{iii}	91.3 (3)	O1—C7—C1	115.7 (11)
O3^{ii}—Cu—O2^{iii}	89.4 (3)	O2—C7—C1	116.1 (10)
O1—Cu—N1^{iv}	99.3 (3)	O4—C8—O3	126.5 (11)
O4^{i}—Cu—N1^{iv}	94.1 (3)	O4—C8—C3	117.4 (11)
O3^{ii}—Cu—N1^{iv}	98.5 (3)	O3—C8—C3	115.6 (11)
O2^{iii}—Cu—N1^{iv}	93.4 (3)	N1—C10—C11	110.4 (10)
C7—O1—Cu	123.6 (7)	N1—C10—C9	120.9 (10)
C7—O2—Cu^{iii}	120.9 (7)	C11—C10—C9	128.4 (10)
C8—O3—Cu^{v}	120.8 (7)	C12—C11—C10	107.5 (10)
C8—O4—Cu^{vi}	125.0 (7)	C12—C11—N3	120.9 (11)
N2—N1—C10	105.6 (9)	C10—C11—N3	131.6 (11)
N2—N1—Cu^{iv}	122.0 (7)	C11—C12—N2	103.2 (11)
C10—N1—Cu^{iv}	132.3 (7)	C11—C12—C13	133.5 (12)
N1—N2—C12	113.3 (10)	N2—C12—C13	123.3 (12)
N1—N2—H2N	123.4	O5—C14—N5	136 (3)
C12—N2—H2N	123.4	O5—C14—H14	112.2
N4—N3—C11	112.8 (10)	N5—C14—H14	112.2
N3—N4—C5	113.9 (10)	C2—C3—C4	118.6 (11)
C14—N5—C15	124 (2)	C2—C3—C8	120.6 (11)

C14—N5—C16	125 (2)	C4—C3—C8	120.8 (11)
C15—N5—C16	111.0 (16)	C5—C4—C3	118.9 (11)
C6—C1—C2	116.4 (12)	C6—C5—C4	121.0 (10)
C6—C1—C7	122.9 (11)	C6—C5—N4	114.6 (10)
C2—C1—C7	120.8 (11)	C4—C5—N4	124.3 (11)
C3—C2—C1	122.6 (11)		

Symmetry codes: (i) x, -y+1/2, z+1/2; (ii) -x, y+1/2, -z+1/2; (iii) -x, -y+1, -z+1; (iv) -x+1, -y+1, -z+1; (v) -x, y-1/2, -z+1/2; (vi) x, -y+1/2, z-1/2.

Table S2. Selected Bond lengths [Å] and angles [°] for [Zn(HIsa-az-dmpz)])]·$(DMF)_2$.

Zn—O1	2.028 (3)	C5—C6	1.377 (5)
Zn—N1^{i}	2.028 (3)	O6—C17	1.273 (10)
Zn—O4^{ii}	2.033 (3)	N6—C17	1.368 (9)
Zn—O2^{iii}	2.033 (3)	N6—C18	1.433 (9)
Zn—O3^{iv}	2.041 (3)	N6—C19	1.399 (10)
O1—C7	1.255 (5)	C9—C10	1.472 (6)
N1—C10	1.337 (5)	C10—C11	1.413 (5)
N1—N2	1.362 (4)	C11—C12	1.388 (6)
C1—C2	1.385 (5)	C12—C13	1.490 (6)
C1—C6	1.396 (5)	O5—C14	1.256(6)
C1—C7	1.503 (5)	N5—C14	1.294 (6)
O2—C7	1.262 (5)	N5—C16	1.445 (7)
N2—C12	1.336 (6)	N5—C15	1.465 (6)
N2—H2N	0.830 (10)	C3—C4	1.409 (5)
C2—C3	1.376 (5)	C3—C8	1.499 (5)
O3—C8	1.255 (5)	O4—C8	1.251 (5)
N3—N4	1.255 (4)	N4—C5	1.444 (5)
N3—C11	1.405 (5)	C4—C5	1.382 (5)
O1—Zn—N1^{i}	102.10 (12)	O4—C8—O3	126.0 (4)
O1—Zn—O4^{iii}	86.95 (12)	O4—C8—C3	116.7 (3)
N1^{i}—Zn—O4^{iii}	102.01 (12)	O3—C8—C3	117.3 (3)
O1—Zn—O2^{ii}	158.03 (11)	N1—C10—C11	108.3 (3)
N1^{i}—Zn—O2^{ii}	99.85 (11)	N1—C10—C9	121.5 (3)
O4^{iii}—Zn—O2^{ii}	89.36 (12)	C11—C10—C9	130.2 (4)
O1—Zn—O3^{iv}	87.16 (11)	C12—C11—N3	120.8 (4)
N1^{i}—Zn—O3^{iv}	100.01 (11)	C12—C11—C10	106.8 (3)
O4^{iii}—Zn—O3^{iv}	157.94 (11)	N3—C11—C10	132.4 (4)
O2^{ii}—Zn—O3^{iv}	88.20 (11)	N2—C12—C11	106.1 (3)
O1—Zn—Zn^{ii}	77.39 (8)	N2—C12—C13	122.3 (4)
N1^{i}—Zn—Zn^{ii}	178.69 (9)	C11—C12—C13	131.6 (4)

O4^{ii}—Zn—Zn^{iii}	76.77 (8)	O5—C14—N5	125.2 (5)
O2^{ii}—Zn—Zn^{ii}	80.68 (8)	O6—C17—N6	124.8 (10)
O3^{iv}—Zn—Zn^{ii}	81.20 (8)	O6—C17—H17	124.7
C7—O1—Zn	130.2 (3)	N6—C17—H17	109.5
C10—N1—N2	107.0 (3)	C14—N5—C16	120.9 (5)
C10—N1—Zn^{i}	131.2 (3)	C14—N5—C15	121.0 (4)
N2—N1—Zn^{i}	121.6 (2)	C16—N5—C15	118.0 (4)
C2—C1—C6	119.0 (3)	C6—C5—C4	120.7 (4)
C2—C1—C7	121.5 (3)	C6—C5—N4	115.0 (3)
C6—C1—C7	119.4 (3)	C4—C5—N4	124.3 (4)
C7—O2—Zn^{ii}	125.6 (2)	C17—N6—C18	121.1 (7
C12—N2—N1	111.7 (3)	C17—N6—C19B	120.2 (8)
C12—N2—H2N	126 (3)	C18—N6—C19B	118.7 (8)
N1—N2—H2N	122 (3)	C5—C6—C1	120.2 (4)
C3—C2—C1	120.8 (3)	O1—C7—O2	125.6 (4)
C8—O3—Zn^{v}	124.8 (2)	O1—C7—C1	116.7 (3)
N4—N3—C11	113.1 (3)	O2—C7—C1	117.7 (3)
C2—C3—C4	119.9 (3)	C8—O4—Zn^{vi}	131.2 (3)
C2—C3—C8	120.5 (3)	N3—N4—C5	112.2 (3)
C4—C3—C8	119.6 (3)	C5—C4—C3	119.2 (4)

Symmetry codes: (i) -x+2, -y, -z+1; (ii) -x+1, -y, -z+1; (iii) x, -y-1/2, z+1/2; (iv) -x+1, y+1/2, -z+1/2; (v) -x+1, y-1/2, -z+1/2; (vi) x, -y-1/2, z-1/2.

References

1 S. L. Xiang, J. Huang, L. Li, J. Y. Zhang, L. Jiang, X. J. Kuang and C. Y. Su, *Inorg. Chem.*, 2011, **50**, 1743-1748.
2 J. F. Eubank, L. Wojtas, M. R. Hight, T. Bousquet, V. C. Kravtsov and M. Eddaoudi, *J. Am. Chem. Soc.* 2011, **133**, 17532-17535.
3 L. Wen, W. Shi, X. Chen, H. Li and P. Cheng, *Eur. J. Inorg. Chem.*, 2012, **2012**, 3562-3568.
4 S.-M. Zhang, Z. Chang, T.-L. Hu and X.-H. Bu, *Inorg. Chem.*, 2010, **49**, 11581-11586.
5 S. Wang, Z.-W. Wei, J. Zhang, L. Jiang, D. Liu, J.-J. Jiang, R. Si and C.-Y. Su, *IUCrJ*, 2019, **6**, 85-95.
6 Y. Xiong, Y. Z. Fan, R. Yang, S. Chen, M. Pan, J. J. Jiang and C. Y. Su, *Chem. Commun.*, 2014, **50**, 14631-14634.
7 Y. Xiong, Y. Z. Fan, R. Yang, S. Chen, M. Pan, J. J. Jiang and C. Y. Su, *Chem. Commun.*, 2014, **50**, 14631-14634.
8 Z. J. Chen, K. Adil, L. J. Weselinski, Y. Belmabkhout and M. Eddaoudi, *J. Mater. Chem. A*, 2015, **3**, 6276-6281.
9 T. L. Hu, H. Wang, B. Li, R. Krishna, H. Wu, W. Zhou, Y. Zhao, Y. Han, X. Wang, W. Zhu, Z. Yao, S. Xiang and B. Chen, *Nat. Commun*, 2015, **6**, 7328.
10 X. Liu, M. Oh and M. S. Lah, *Cryst. Growth Des.*, 2011, **11**, 5064-5071.
11 Q. Wang, J. Jiang, M. Zhang and J. Bai, *Cryst. Growth Des.*, 2016, **17**, 16-18.
12 K. Kobalz, M. Kobalz, J. Möllmer, U. Junghans, M. Lange, J. Bergmann, S. Dietrich, M. Wecks, R. Glaser and H. Krautscheid, *Inorg. Chem.*, 2016, **55**, 6938-6948.
13 F. R. Japp and F. Klingemann, F. Liebigs Ann. Chem. 1888, **247**, 190-225.
14 M. N. Kopylovich, M. J. Gajewska, K. T. Mahmudov, M. V. Kirillova, P. J. Figiel, M. F. C. Guedes da Silva, B. Gil-Hernandez, J. Sanchiz and A. J. L. Pombeiro, *New J. Chem.*, 2012, **36**, 1646-1654.
15 Mercury CSD 4.1, Program for Crystal Structure Visualisation, Exploration and Analysis from the Cambridge Crystallographic Data Center, Copyright CCDC 2001-2016, http://www.ccdc.cam.ac.uk/mercury/
16 C. F. Macrae, I. J. Bruno, J. A. Chisholm, P. R. Edgington, P. McCabe, E. Pidcock, L. Rodriguez-Monge, R. Taylor, J. van de Streek and P. A. Wood, *Journal of Applied Crystallography*, 2008, **41**, 466-470.
17 A. Spek, *Acta Crystallographica Section D*, 2009, **65**, 148-155.
18 PLATON – A Multipurpose Crystallographic Tool, Utrecht University, Utrecht, The Netherlands, A. L. Spek (2008); Windows implementation: L.J. Farrugia, University of Glasgow, Scotland, Version 40608, (2008).
19 CrystalExplorer17, Version 3.1; Turner, M. J.; McKinnon, J. J.; Wolff, S. K.; Grimwood, D. J.; Spackman, P. R.; Jayatilaka, D.; Spackman, M. A.: University of Western Australia, 2017. http://hirshfeldsurface.net
20 M. J. Turner, J. J. McKinnon, D. Jayatilaka and M. A. Spackman, *CrystEngComm*, 2011, **13**, 1804-1813.
21 L. Gurvich, *J. Phys. Chem. Soc. Russ.,* 1915, **47**, 805-827.
22 V. A. Blatov, A. P. Shevchenko and D. M. Proserpio, *Cryst. Growth. Des.*, 2014, **14**, 3576-3586.